Spatial and temporal evolution of horizontally extensive lightning discharges associated with sprite-producing positive cloud-to-ground flashes in northeastern Spain.

O.A. van Der Velde, J. Montanya, S. Soula, N. Pineda, J. Bech

Spatial and temporal evolution of horizontally extensive lightning discharges associated with sprite-producing positive cloud-to-ground flashes in northeastern Spain

Oscar A. van der Velde,[1] Joan Montanyà,[1] Serge Soula,[2] Nicolau Pineda,[3] and Joan Bech[3]

Received 30 August 2009; revised 21 April 2010; accepted 26 April 2010; published 28 September 2010.

[1] During the evening of 6 August 2008, a small mesoscale convective system (MCS) entered the area of radar and 2-D interferometric lightning detection system coverage in northeastern Spain and produced 17 sprites recorded by a camera at only 95–180 km distance. This study presents an analysis of the in-cloud component of the sprite-associated lightning flashes and those of other flashes. The analysis focuses on the horizontal development of sprite-producing lightning by discussing three examples, divided into the periods before the positive cloud-to-ground flash (+CG), between +CG and the end of the sprite, and the period after the sprite. Location and horizontal size of sprites appear to be well explained by the temporal and spatial development of the lightning path. The majority of sprite-producing discharges started directly at the rear side of developing and mature convective cores within the decaying MCS, either with the +CG or with preceding negative leaders. The +CG started a burst of VHF sources during which the sprite developed. Delayed carrot sprites developed after a secondary, smaller burst and were well collocated with the burst toward the rear of the MCS. The order of development of elements in a grouped sprite followed the direction of lightning propagation during the burst stage. The second part of the analysis concentrates on the metrics of sequences of VHF sources and shows that sprites are indeed produced by the largest, longest lasting discharges with particularly large line-perpendicular dimensions (37 km median compared with 11 km for +CG >25 kA).

Citation: van der Velde, O. A., J. Montanyà, S. Soula, N. Pineda, and J. Bech (2010), Spatial and temporal evolution of horizontally extensive lightning discharges associated with sprite-producing positive cloud-to-ground flashes in northeastern Spain, *J. Geophys. Res.*, *115*, A00E56, doi:10.1029/2009JA014773.

1. Introduction

[2] It has been 20 years since peculiar optical flashes in the clear sky above thunderstorms were recorded and confirmed for the first time [*Franz et al.*, 1990]. Sprites, as they were called 5 years after their discovery, occur at altitudes between 40 and 90 km in the mesosphere [*Sentman et al.*, 1995] a few milliseconds to tens of milliseconds after intense positive cloud-to-ground flashes (+CG) [*Boccippio et al.*, 1995; *Lyons et al.*, 2003]. Only very few −CG-triggered sprites have been reported [*Barrington-Leigh et al.*, 1999; *Williams et al.*, 2007]. +CG flashes support continuing currents up to a few kiloamperes (kA) which can last a few hundred milliseconds [e.g., *Rust et al.*, 1985; *Bell et al.*, 1998; *Cummer and Füllekrug*, 2001; *Füllekrug et al.*, 2006; *Campos et al.*, 2009], so that large amounts of charge can be drained from the cloud. In response to the charge removal, a transient electric field develops between the cloud and the ionosphere. *Pasko et al.* [1996] explained that the effect of a sudden removal of positive charge from the thunder cloud is equivalent to inserting negative charge of the same magnitude, so that the resulting quasi-electrostatic field in the mesosphere causes streamers of positive polarity to grow downward and negative streamers to grow upward. Details of sprite development are currently being unraveled by analysis of high-speed camera recordings [e.g., *Cummer et al.*, 2006; *McHarg et al.*, 2007, *Montanyà et al.*, 2010].

[3] So far the only way to approximate the strength of the quasi-electrostatic field has been via remote recordings of extremely low frequency radio (ELF) waves by calculating the impulse charge moment change [e.g., *Huang et al.*, 1999; *Hu et al.*, 2002; *Cummer and Lyons*, 2005; *Greenberg et al.*, 2007, 2009]. For longer lasting discharges, the dielectric relaxation due to conductivity of air significantly counteracts the effects of ongoing charge removal. The total charge moment change values can then become very large, but the corresponding electric fields become just large enough to trigger a long-delayed sprite [*Li et al.*, 2008; *Hu et al.*, 2007]. Most sprites are delayed up to 10–20 ms to their associated

[1]Lightning Research Group, Electrical Engineering Department, Technical University of Catalonia, Terrassa, Spain.
[2]Université de Toulouse, Laboratoire d'Aérologie, CNRS, Observatoire midi-Pyrenées, Toulouse, France.
[3]Meteorological Service of Catalonia, Barcelona, Spain.

0148-0227/10/2009JA014773

+CG, with relatively few sprites delayed longer than 40 ms [*São Sabbas et al.*, 2003]. However, *Mika et al.* [2005] found 35% of sprites to be long-delayed (30–280 ms), and there are studies which have found much longer average delays for winter sprites over maritime storms [65–85 ms, *Greenberg et al.*, 2007; 45–90 ms depending on geographic region, *Matsudo et al.*, 2009]. Generally, delays of 200–400 ms can be considered exceptional. The horizontal displacement of the sprite to the triggering +CG can be greater than 50 km, consistent with previous studies by *Lyons* [1996] and *Wescott et al.* [2001]. This horizontal displacement could be partially due to charge removal by horizontally extensive in-cloud lightning channels away from the +CG stroke, which was tentatively confirmed by our initial case study [*Neubert et al.*, 2008, section 2.2] and partially due to other factors determining ionization in the mesosphere. Occasionally, displaced sprites have their lower tendrils apparently aligned with the electrical field lines from the region of charge removal [*Neubert et al.*, 2005]. Also, *Vadislavsky et al.* [2009] described the occurrence of ringlike grouping regularly observed in columniform sprites, and *Stanley* [2000] noted that the elements of grouped sprites appeared to occur at the perimeter of the associated mapped lightning flashes. It has been speculated that radiated electric fields of the in-cloud discharge or electromagnetic interference patterns cause important ionization [*Valdivia et al.*, 1997; *Cho and Rycroft*, 2001] on top of the quasi-electrostatic fields, but also gravity waves [e.g., *Pasko et al.*, 1997; *Sentman et al.*, 2003] or any other preexisting ionization patterns (sometimes visible as structured sprite halos [*Moudry et al.*, 2003]) have been considered to influence the spacing of sprite elements. Furthermore, *Yashunin et al.* [2007] calculated that surges in continuing current in vertical lightning channels enhance the quasi-electrostatic field laterally.

[4] Very low frequency (VLF) radio sferic clusters suggest that strong in-cloud lightning activity is indeed associated with sprites [*Ohkubo et al.*, 2005; *van der Velde et al.*, 2006]. The first direct mapping of in-cloud lightning channels associated with sprite-producing CG flashes was provided by *Stanley* [2000] and *Lyons et al.* [2003]. *Marshall et al.* [2007] confirmed VLF sferic clusters to correlate strongly with directly detected in-cloud lightning channels, which were confirmed to be an important component of sprite-producing discharges, but the VLF sferic cluster signature is not unique to sprites.

[5] The type of thunderstorm most commonly associated with sprites is the Mesoscale Convective System (MCS) during the mature to decaying stage [*Lyons*, 1996]. During these stages, a wide area of light to moderate "stratiform" precipitation has developed adjacent to the more intense convective cores, which are often arranged linearly. The stratiform region contains extensive layers of alternating charge polarity at different altitudes [e.g., *MacGorman and Rust*, 1998]. This part of the MCS has lower CG flash rates than the cores, of predominately positive polarity, and produces large horizontal discharges known as spider lightning [e.g., *Mazur et al.*, 1998; *Lang et al.*, 2004], which often are directed from the higher altitudes of convective regions toward lower altitudes in the stratiform region, supposedly following trajectories of ice particles toward the rear of the storm system [*Carey et al.*, 2005; *Ely et al.*, 2008]. These horizontally extensive lightning flashes can have multiple connections to ground of different polarity [*Lang et al.*, 2004]. *Soula et al.* [2009] described sequences of several CGs in particular for sprite-producing flashes in France, and it was suspected they were either connected by long horizontal lightning channels or triggered indirectly by electric field changes, much like independent storm cells can exhibit "communicating" lightning flashes [*Yair et al.*, 2006, 2009].

[6] *Mazur* [2002] summarized the development and different processes of lightning flashes. It is widely believed that lightning (with the exception of upward discharges from objects connected to the ground) develops as a bidirectional leader [*Kasemir*, 1960] in a region of the cloud where the electric field strength has been observed to surpass the runaway breakdown threshold [*Stolzenburg et al.*, 2007], commonly between two charged areas in the cloud. The negative leader end builds in the direction of positive charge and usually displays a stepped behavior. The positive leader end grows toward negative charge and usually does not step. Recoil streamers, now called recoil leaders [*Mazur*, 2002], are of negative polarity and connect repetitively to the positive leader end, extending the channel retrogressively at speeds of 2×10^4 m s^{-1} [*Proctor et al.*, 1988; *Shao and Krehbiel*, 1996]. The positive leader itself moves commonly at speeds between 0.3–6 $\times$ 10^5 m s^{-1} (vertically [*Saba et al.*, 2008, *Kong et al.*, 2008]). Negative leaders propagate at similar speeds, on average 2×10^5 m s^{-1} [e.g., *Mazur et al.*, 1998; *Morimoto et al.*, 2005]. Recoil leaders are very fast processes with minimum observed speeds of 4×10^6 m s^{-1} [*Saba et al.*, 2008] to several 10^7 m s^{-1} [e.g., *Richard et al.*, 1986; *Rhodes et al.*, 1994].

[7] In this article, we demonstrate the development of lightning discharges that produced +CG flashes which triggered sprites by means of an interferometer network which provides two-dimensional maps of VHF sources. Additionally, we demonstrate by means of a statistical study the extent to which the sprite-producing flashes are different from other flashes.

2. Data

[8] The storm chosen for this work occurred during the evening of 6 August 2008 and produced 17 sprites when it was within range of the interferometric lightning detection system operated by the Meteorological Service of Catalonia in northeastern Spain [*Montanyà et al.*, 2006]. This system consisted of two SAFIR (Système d'Alerte Foudre par Interférométrie Radioélectrique [*Richard and Lojou*, 1996]) and two upgraded sensors (LS8000), processed by a more recent CP8000 central processor (Vaisala, Inc.). This system computes azimuthal (two-dimensional) directions from each antenna site to sections of a lightning flash by analyzing phase differences between antenna pairs of bursts of very high frequency (VHF) radio pulse trains and provides locations and times of all located radio sources. The time resolution is 10^{-4} second. Triangulation from the four sensor sites (marked in Figure 1) is possible if at least two sensors were able to detect and correlate the radio emissions from the lightning flash. The detection range extends ~250 km from the center of the network, but low altitudes in the storm at shorter distances may be blocked by the local horizon at the sensor locations. The azimuthal precision of the sensors is specified as 0.5° RMS. For this storm, most sources were

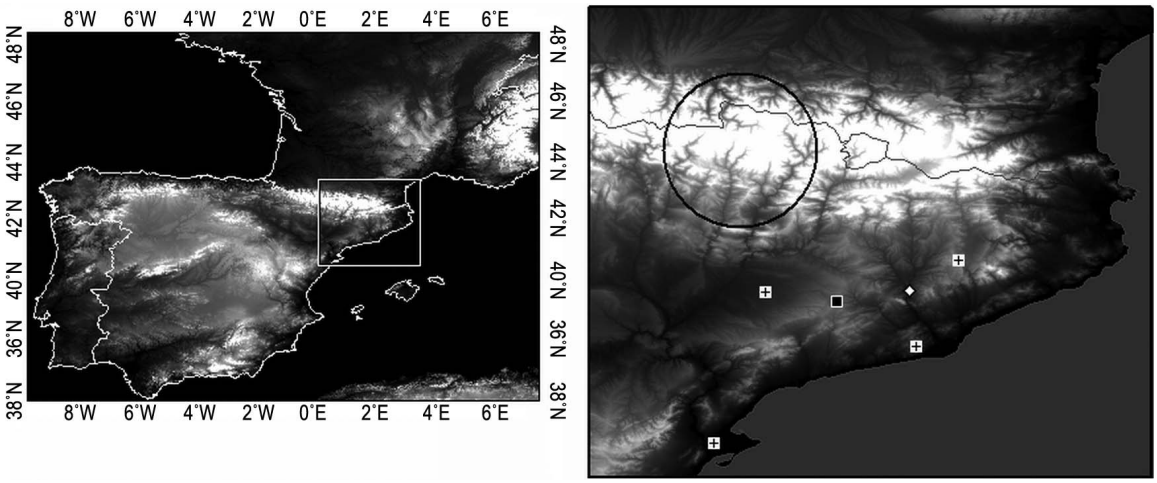

Figure 1. Map of Spain and the region concerned in this study. The radar is plotted as a black square, XDDE (Xarxa de Detecció de Descàrregues Elèctriques) stations as crosses, and the camera as a diamond, with the region of interest in a black circle.

located only by two sensors. For this study, the CG information from the system was not used, only the VHF sources. Since the configuration of the system and the resulting detection efficiency characteristics may be particular to this region, we refer to the data as XDDE (Xarxa de Detecció de Descàrregues Elèctriques), the abbreviation in use by the regional weather service.

[9] CG stroke locations, times, and peak current information were provided by the LINET network (Lightning Network), which utilizes direction finding and time of arrival in very low to low radiofrequency range [*Betz et al.*, 2004] and which has in recent years expanded to southern France and northern Spain. LINET detects a greater number of CGs related to sprite-producing flash sequences than the EUCLID (European Cooperation for Lightning Detection) network for the region surrounding the Pyrenees. In EUCLID, several Vaisala-manufactured national networks are joined, such as Météorage in France, used in *van der Velde et al.* [2006]). It is the European equivalent of the North American Lightning Detection Network (NALDN). An estimate of detection efficiency (DE) for sprite-triggering +CG flashes for nine recent storms in northeastern Spain and southern France including 188 sprites yielded for LINET a DE of 93%, whereas EUCLID obtained a DE of 76%. The peak current values of LINET are usually quite close to those of EUCLID (within 5%–15%).

[10] C-band radar 0.6° Plan Position Indicator (PPI) scans from the radar of Panadella (marked in Figure 1) in central Catalonia, available at 6-minute intervals, were used to describe the structure and development of the thunderstorm system. Radar images were georeferenced, allowing comparisons with lightning locations.

[11] Sprites were observed using a Watec 902H2 Ultimate camera operated in Sant Vicenç de Castellet (41.67°N, 1.86°E, marked in Figure 1) with a manual gain setting and a CBC Computar 12 mm F0.8 lens with a horizontal field of view of 31°. Its interlaced video fields provided a time resolution of 20 ms (PAL standard). The capturing of events was done with UFOCapture software. In the audio track of the video clips, the sferics received by two AM (amplitude modulation) radios, tuned to approximately 150 kHz and 1650 kHz, were recorded. Although this data is unsuitable for quantitative purposes (polarity cannot be retrieved, gain and filtering are unknown), it lends itself well to a qualitative comparison of the lightning detection systems and the sferic bursts, particularly with respect to the continuity and duration of lightning discharge processes. The presented waveform comes from the radio tuned to approximately 1650 kHz (medium wave, MW), with a passband of 4.5 kHz. Noise reduction was applied.

[12] Initially, a target storm was over southwestern France, but the thunderstorm system described in this study traveled between the observer and the French storm. The first sprite was recorded over this storm at 2056 UT in the top left corner of the image, requiring adjustment of the camera's view. The sprites were then successfully followed during more than an hour, with distances from the observing site of only 95–180 kilometers. Owing to the short distance, the semitransparent anvil cloud of the storm interfered with the observations, in particular between 2130 and 2145 UT, and it is possible that sprites occurring over the far end of the storm were invisible. From the stars visible in the images, accurate azimuths and elevations were retrieved by means of star catalog software which allows fitting the stars to a background image of the sprite after rescaling the PAL 720 × 576 pixels images to a 4:3 aspect ratio. The great circle paths from the camera to the sprite elements (the features marked by crosses in Figure 2) have been plotted to a maximum distance corresponding to an altitude of ~85 km. Sprites are commonly reported to initiate between 70 and 85 km altitude [e.g., *Cummer et al.*, 2006; *McHarg et al.*, 2007], which is also roughly the altitude of the visually identifiable transition region between downward streamers and diffuse upper parts [*Pasko et al.*, 1998]. If we take 70 km as the altitude for a reasonable lower bound on the

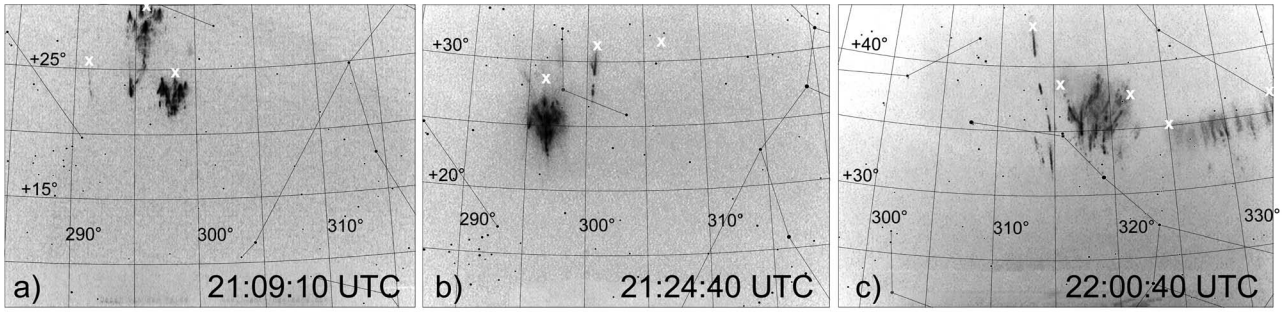

Figure 2. Inverted images of the three example sprite events of 2109:10, 2124:40, and 2200:40 UTC with a grid overlay of azimuth and elevation, based on matching stars in the image and software. The sprite features marked by white crosses are indicated by great circle paths mapped in Figure 3, 4, and 5, respectively. (a) The double carrot sprite event of 2109:10. The lower marked column and carrot, including the column between them, occurred between 101–141 ms, while the carrot near the top edge of the image occurred between 501–541 ms. (b) The carrot sprite event of 2124:40. The two small elements at the right were weakly luminous between 032–178 ms, while the carrot near the top edge of the image occurred after a long delay, between 178–198 ms. (c) The sprite event of 2200:40. The sprite started at the right side of the image in the first frame (40.976–41.016 s), then developed the central part during subsequent frames (40.996–41.036 s), followed by its decay, while the columniform filaments at the left side developed slightly later (41.036–076 s) and decayed very slowly, with upward-moving luminous parts.

distance, the resulting locations would be ~20 km closer to the camera as an indication of the location precision.

3. Methods

[13] The original XDDE source locations per flash can look rather incoherent and often appear in radial patterns caused by random noise and azimuthal digitization. This is worse at larger distances from the baselines between sensors and when the angle of a lightning VHF emission to the baseline between two sensors is small. The system itself provides confidence ellipses on the basis of the azimuthal errors of the sensors. The mean dimension of the longest ellipse axis for 95% probability is 19.5 km with a standard deviation of 13.8 km. For the shortest ellipse dimension, these numbers are 6 km and 2.2 km, respectively. The mean ellipse axis orientation is 127° with a standard deviation of 27°. So, the position error is most severe in a direction along the linear MCS, which is oriented on average along 150°.

[14] While plotting the data, time-coloring the sources allows one to follow the progress of the discharge, even when subsequent sources show erratic behavior in the spatial domain. For the statistical study, a moving average (running mean) with a window of six subsequent sources was performed on latitude and longitude data, which resulted in much more consistent patterns which are less dispersed radially. The window size was essentially an arbitrary choice. Visually, the moving average of six worked best. An assessment of the spatial scatter before and after the moving average procedure has been done on the basis of the source-to-source distance within groups of sources with intersource time interval of <0.2 ms, close to the resolution of the XDDE system. The data show that 95% of raw source-to-source distances are <24 km, whereas the moving average with a window of six results in 95% of source-to-source distances <3.3 km. The resulting cluster size of sources is reduced from 95% <37 km to <15 km. Using a wider window for the moving average does not decrease this further. At the same time, the median speed between sources separated in time by at most 300 ms is 1.1×10^7 m s^{-1} in the raw data, which is reduced to 2.4×10^5 m s^{-1} after the moving average in space and time domains (standard deviation 5×10^4 m s^{-1} to 4×10^6 m s^{-1}), corresponding to common values quoted for negative leaders. The choice of a window of 5 or 7 points leads to ~20% larger or 10% lower source-to-source distances and speeds, respectively, and similar differences in sequence size. Although the propagation speeds are in correspondence with reported values, we must remember that they are not a result of real measured leader propagation or other process velocity, because these cannot be inferred from the data. For this reason, apparent propagation speeds are not considered.

[15] In particular for the statistical part of this study, XDDE data were organized into "sequences" (a proxy for flashes) on the basis of a time criterion that groups original VHF sources if they occur within 300 ms of each other. The threshold is close to the typical criterion for CG lightning detection networks to group strokes belonging to flashes. Video observations of interstroke intervals show that this criterion is very suitable [e.g., *Valine and Krider*, 2002; *Saba et al.*, 2006]. However, this interval is a trade-off between including sources which could belong to the same flash and excluding sources which belong to different flashes. This is mostly (but not exclusively) a problem at high flash rates. A distance criterion was not applied because the individual raw source locations, ordered by time of occurrence, were too noisy. An advanced grouping algorithm would be required to deal with this, which would have made the procedure (and hence the results of the statistical analysis) less transparent and no less dependent on the choice of grouping criteria.

[16] Finally, the word *burst* is used throughout the text. It is loosely defined as a series of VHF sources, usually >10, with typically submillisecond time intervals between sour-

Table 1. Time Evolution of Convective Cores of the MCS After Breakup of the Original Convective Line, and the Sprite Events Which Were Triggered by Lightning Initiating at the Corresponding Cores

Core	Start time	Time of maximum reflectivity	End time	Related Sprites
A	2106	2124	2136	2109, 2112, 2115
B	2054	2112	2142	2056, 2059, 2100, 2110, 2111, 2117
C	2124	2142	2154	2131, 2146
D	2118	2130	2142	2119, 2124
E	2136	2142	2200	2156, 2200, 2203

ces, in contrast with more isolated VHF sources with much longer intervals (tens of milliseconds).

4. Evolution of the Mesoscale Convective System

[17] At 2000 UT, the radar network of the Catalonian weather service scanned a 67-km-long and 14-km-wide northwest-southeast-oriented linear multicell thunderstorm with strong precipitation intensity values (50–60 dBZ radar reflectivity) entering the region. The storm developed in the afternoon over central Spain and moved in a north-northeasterly direction. Surrounding weaker precipitation became visible near the northwestern end of the line. After 2024 UT, the northwestern half of the line started to lose intensity (from >50 dBZ to 35–45 dBZ), followed shortly by a weakening and disorganization of the southern half of the line, especially after 2048 UT. After the convective line broke up and during the expansion of stratiform precipitation, the total flash rates detected by XDDE decreased steadily while the number of +CG flashes with high peak currents increased.

[18] The system assumed a weak (broken) leading line-trailing stratiform structure, which measured a maximum 70 km front to rear ~2130 UT. The convective line became interrupted by areas of reflectivity of 25–35 dBZ after 2100 UT. The first sprite was recorded during this stage at 2056 UT, although earlier sprites may have occurred when the camera was still observing the larger, more distant MCS over southwestern France. The fragmented convective region contained several persistent maxima of higher reflectivity, labeled as core A, B, C, D, and E by order of direction (NW to SE). These cores were actually *not* just remains of the convective line, but were growing and decaying in an independent fashion.

[19] Core A developed in advance of the stratiform precipitation NW of the original line, and reached the strongest reflectivity at 2124 UT. It was near the limit of the radar range. Core B at first sight appeared as a surviving group of cells from the northwestern part of the line, but closer inspection revealed it developed newly ahead of the line, which then decayed behind it. This core was the largest and longest lasting. It started to weaken after 2118 UT while a small new core C grew directly at its east flank, which obtained its strongest reflectivity at 2142 UT and then decreased. Behind core B and C, the widest and most intense stratiform precipitation region (moderate, relatively uniform precipitation) developed. The southeastern half of the original line fragmented at 2118 UT, with core D developing in advance of the further decaying line. Core D still increased in intensity until 2130 UT and was overtaken by a newly developed core E just to its east at 2142 UT. Core E retained reflectivity values over 35 dBZ until 2200 UT. The rest of the line segment to the southeast disappeared in the meantime. The extent of the stratiform precipitation area directly behind cores D and E was not much wider than the original convective line, at least at low altitudes.

[20] These cores appeared to be a starting point of sprite-producing discharges, as the examples in the following section show. Table 1 summarizes the life cycles of the convective cores and the associated sprites, of which the lightning discharge or +CG initiated at the corresponding core. The occurrence of sprites in space and time appeared closely tied to the presence of these cores, and the period before the maximum precipitation intensity of the core at the ground is the prime time for initiating sprite-producing discharges (except for core E). So, the decay of large parts of convective areas with simultaneous expansion of stratiform precipitation area introduces a period of sprites, which were triggered by lightning flashes initiating in or near convective cores in their growing stage.

5. Examples of Lightning Sequences Associated With Sprites

[21] We now discuss three examples of the lightning flashes detected by the XDDE and LINET and differentiate between the period before the +CG return stroke, the period between the +CG and the end of the sprite, and the period after the sprite. The examples show the typical characteristics of the discharges but also the limitations of the present XDDE lightning detection system.

5.1. Example 1: 2109:10 UT

[22] This event was the fourth recorded sprite over this thunderstorm and occurred at 2109:10 UT. It consisted of two carrot sprites (Figure 2a) widely separated in time: 101–141 and 501–541 milliseconds. Figures 3 shows the spatial and temporal evolution of the sequence of lightning detections. An initial +CG of 70 kA was detected at 2109:09.907 UT but resulted in only three detected sources and did not (or not immediately) produce the sprite. The +CG that produced the first sprite was detected at 2109:10.111 ms and had a peak current of 46 kA. The location was within 5–10 km of the first +CG. Figure 3 shows the location of sources and the great circle paths to the main sprite elements. The +CG flash producing the sprite occurred at the northern extent of the discharge. At the time of this +CG, a burst of 16 VHF sources was detected, located southwest of the +CG, lasting a few milliseconds. The first sprite was delayed by at most 9 ms. The carrot sprite element did not occur directly over this in-cloud activity but was displaced laterally by at least 19 kilometers from the +CG and by 7 km from the southwestern-most detected in-cloud activity. However, two other simultaneous, smaller elements were even more displaced to the southwest, up to 40 km from the +CG. Lightning activity also occurred directly under the area of the sprites, but this activity was detected *after* the sprite had already decayed, during the period leading to the second sprite 400 ms later.

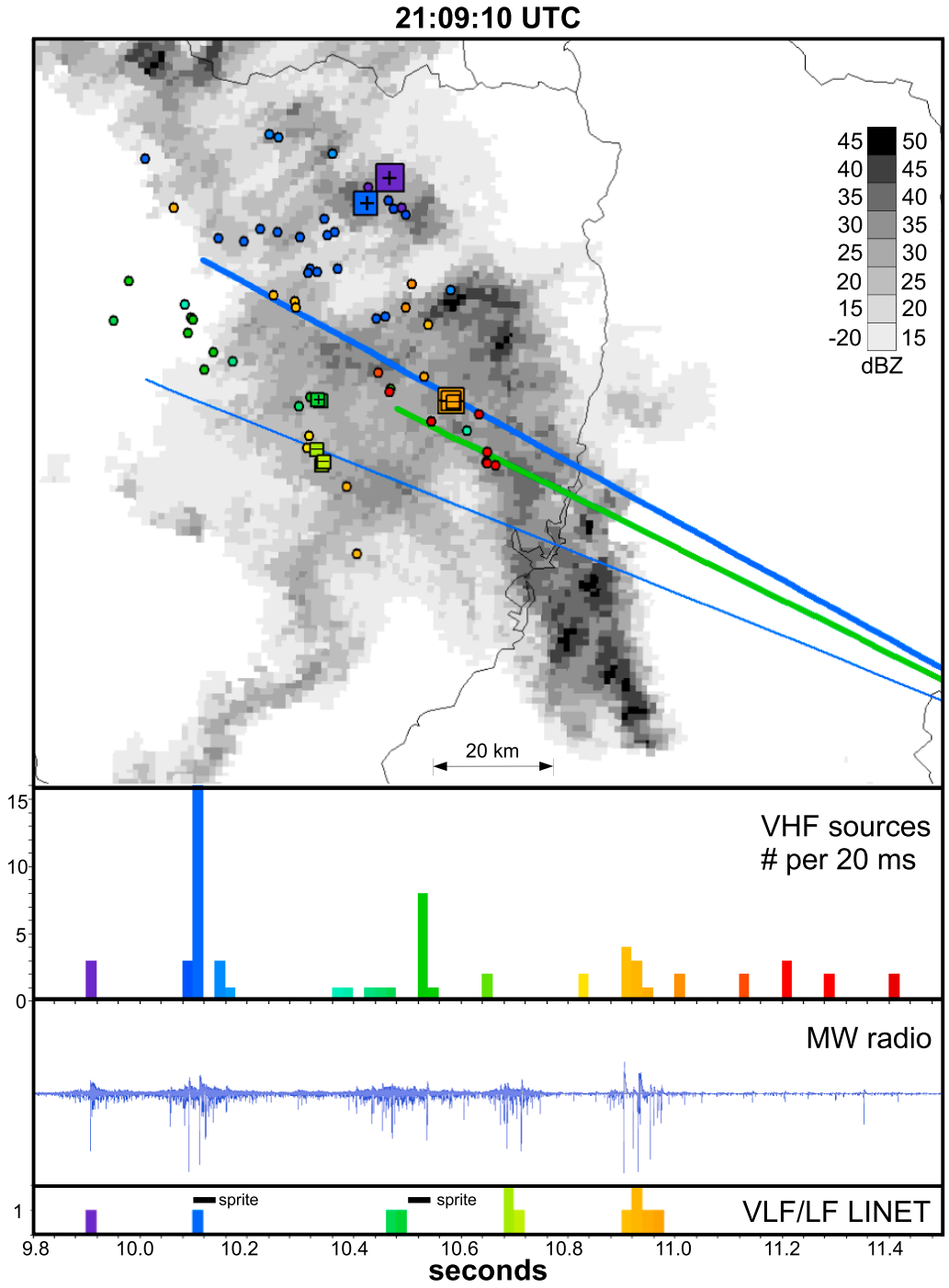

Figure 3. Spatiotemporal representation of detected lightning sources and sprites for the event of 2109:10 UTC. The background is the radar reflectivity image of 2106 UTC. The time evolution of XDDE very high frequency (VHF) sources (circles) and the LINET network (Lightning Network) positive cloud-to-ground flash (+CG) and −CG (+ and − squares) is indicated by symbol color according to the lower images, with a resolution of 20 ms. Square size scales with peak current (see section 5.1 for details). Lines indicate the great circle paths from the camera to the sprite features marked in Figure 2a. The line ends correspond to an assumed sprite feature altitude of 83–87 km. The medium wave radio sferic shows the continuity of the lightning flash as reference. The period covered by this graph spans 1.7 sec with ticks spaced every 40 ms.

[23] Two possible +CGs were detected at 21:09:10.471 and 21:09:10.483 by LINET before the second sprite with peak currents of only 7 and 6 kA with the sprite occurring at a delay of 18–51 ms. However, these weak detections might have been related to M-components (a peak of current superimposed on continuing current as described in +CG flashes, for example, by *Campos et al.* [2009] and *Li et al.* [2008]). So, it is possible that continuing current lasted for more than 400 ms after the first sprite-producing +CG. A second small burst of 9 VHF sources occurred during the progress of the second sprite (at 535 ms, lagging the small +CGs detected by LINET). While the second carrot occurred in the direction of this activity (at a greater elevation in the image), it is impossible that it occurred directly over it because a plausible altitude of the measured sprite initiation point elevation results in a location more to the east. This places the sprite at least 30 km closer to the camera than the VHF sources that occurred around the time of this sprite. After the second sprite, VHF sources occurred scattered over the stratiform area during the following 600 ms. During this period, LINET detected a low peak current −CG with three strokes in the west side of the stratiform region, and a 5-stroke −CG flash at 21:09:10.903–21:09:10.969 with a peak current of −65 kA. The in-cloud detected VHF activity was spatially poorly correlated to these CGs. Finally, the medium wave radio sferic shows that XDDE detections match with several sferic maxima, but reveals also that VHF sources are missing during weaker sferic activity.

[24] Peculiarly, both the first and the second sprite of this event occurred horizontally offset from preceding or simultaneous VHF sources, to the southwest and southeast, respectively. We offer a possible explanation in section 7.

[25] Comparison of the propagation of the lightning sources with the radar image (Figure 3) shows initiation near convective core A at the front side of the system, more to the northwest than the sprites of 2056 and 2059 UT. The sprites occurred over a wide area with more intense moderate (stratiform) reflectivity behind core A and B, and the average path of the flash (not shown) apparently circled the region of weak reflectivity between core A and the second sprite.

[26] In summary, the detected activity can explain the horizontal displacement of the sprite with respect to the triggering +CG, and bursts occur during the sprite appearance and can explain the delay.

5.2. Example 2: 2124:40 UT

[27] The eleventh sprite consisted of a carrot and a long narrow element (Figure 2b), between 21:24:40.178–21:24:40.198 ms. However, at second inspection, one can find a few marginally visible small sprite elements to the right which started at 0.032 and stayed weakly luminous until the carrot sprite appeared. Figure 4 shows the spatial and temporal evolution of the sequence of lightning detections. The +CG that produced the sprite was detected at 21:24:40.020 ms and had a peak current of 31 kA. The carrot sprite was long delayed to this +CG by 158–178 ms. Lightning was detected by the XDDE system 2 sec before the sprite and can be considered as part of the same flash, since the typical intervals between lightning flashes were very long and the radio sferic also shows no interruption longer than 10–20 ms for the entire 2.8 sec displayed in Figure 4. The initial activity was located in a cluster of sources centered on convective core C. At the beginning of the discharge, LINET detected a +5 kA CG (or IC) at 38.695 corresponding well with the location of in-cloud sources. More than 300 ms later, a VHF burst occurred at 39.028–39.033 sec and occurred simultaneously with an optical flash in the video. The burst itself was located 12 km to the west of the initial LINET detection. Some subsequent VHF detections corresponded with weak fluctuations of brightness in the video, after which a second distinct burst at 39.669 sec coincided again with a brighter flash in the video. The detected in-cloud activity then moved to the west, where the sprite-triggering +CG struck in weaker precipitation intensity (the transition region of the MCS). Thirty-four sources followed directly within 10 ms. The activity discharged a region behind convective cell B (in the sense of storm motion), then moving on into the stratiform region toward the rear of the area with reflectivity values >30 dBZ, where six VHF sources were detected during the development of the carrot sprite. From the perspective of the camera and the plausibility of the altitude of the sprite corresponding to that distance, the sprite appears well collocated with the VHF activity. Starting 120 ms after the sprite, LINET also detected five low peak current flashes in the same area of negative polarity over the course of 600 ms. These were marked as "intracloud," at altitudes of 10–15 km (we cannot confirm whether these high values are correct). This activity occurred either as a continuation of the in-cloud leaders or in response to electric field changes resulting from the charge removal that caused the sprite. XDDE also produced a number of sources in this region at that time. Medium wave radio sferics also clearly showed a continuing sferic after the sprite, supporting the continuing leader activity.

5.3. Example 3: 2200:40 UT

[28] The sixteenth sprite occurred at 22:00:40 and consisted of a curtain-like feature at the right side of the image (Figure 2c), visible between 976–1036 ms, followed by a closer appearing, more complex part to the left between 996–1056 ms, slowly decaying. Figure 5 shows the spatial and temporal evolution of the sequence of lightning detections. Note that the graph has been plotted with a fine time resolution 2 ms instead of 20 ms as in the previous two cases. The +CG that produced the sprite was detected at 22:00:40.979 ms and had a peak current of 78 kA (92 kA in EUCLID). The onset of the sprite was delayed by at most 17 ms. VHF sources were first registered by XDDE 62 ms before the +CG (40.916 sec, blue in the color graph), simultaneous with a subtle increase of brightness visible in the video. LINET (but not EUCLID) shows a coincident detection marked as "intracloud" but having a peak current of −19 kA, 2 km south of the later +CG. The radio sferic also shows a marked spike. The initial burst detected by XDDE occurred near core D, well away from the larger region of moderate reflectivity which produced earlier sprites. Note that the northwest-southeast alignment of sources is likely the result of the asymmetric location accuracy as discussed in section 3. The radio sferic actually reveals that a lightning process was going on between the initial detection and the +CG. At the time of the +CG, a

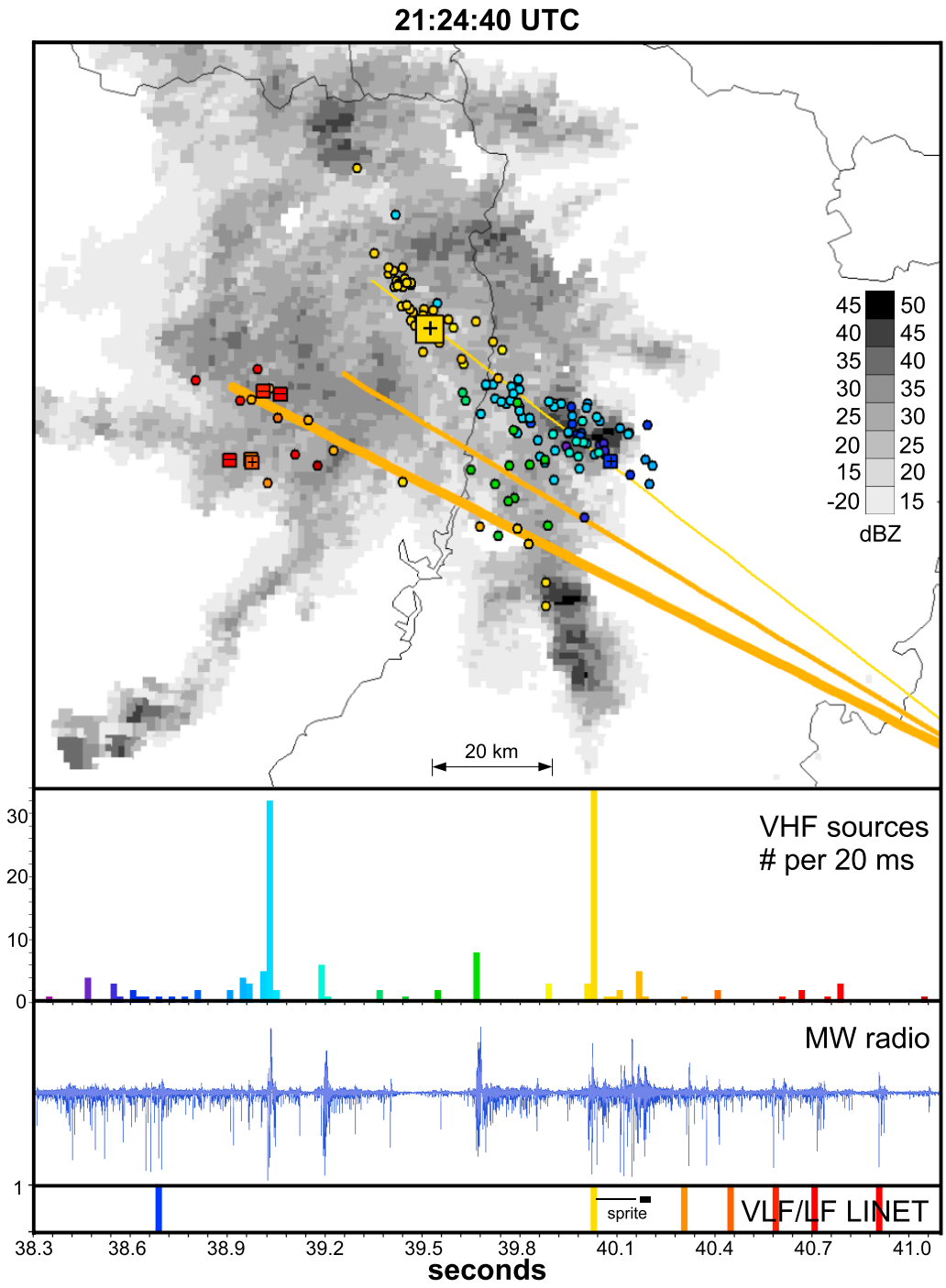

Figure 4. Spatiotemporal representation of detected lightning sources and sprites for the event of 2124:40 UTC. The background is the radar reflectivity image of 2124 UTC. The time evolution of XDDE VHF sources (circles) and LINET +CG and −CG (+ and − squares) is indicated by symbol color according to the lower images, with a resolution of 20 ms. Square size scales with peak current (see section 5.2 for details). Lines indicate the great circle paths from the camera to the sprite features marked in Figure 2b. The line ends correspond to an assumed sprite feature altitude of 83–87 km. The medium wave radio sferic shows the continuity of the lightning flash as a reference. The period covered by this graph spans 2.8 sec with ticks spaced every 60 ms.

burst was detected of 298 VHF sources, lasting until 41.032 sec (52 ms long). This is the largest and most consistent VHF cluster observed, stretching over an area of 27 km, to the southeast and southwest of the +CG. The high number of sources over a large area is likely the result of improved detection efficiency at closer range to the XDDE system (the sprite/lightning event occurred more than 1° longitude to the east of the first events). The VHF burst

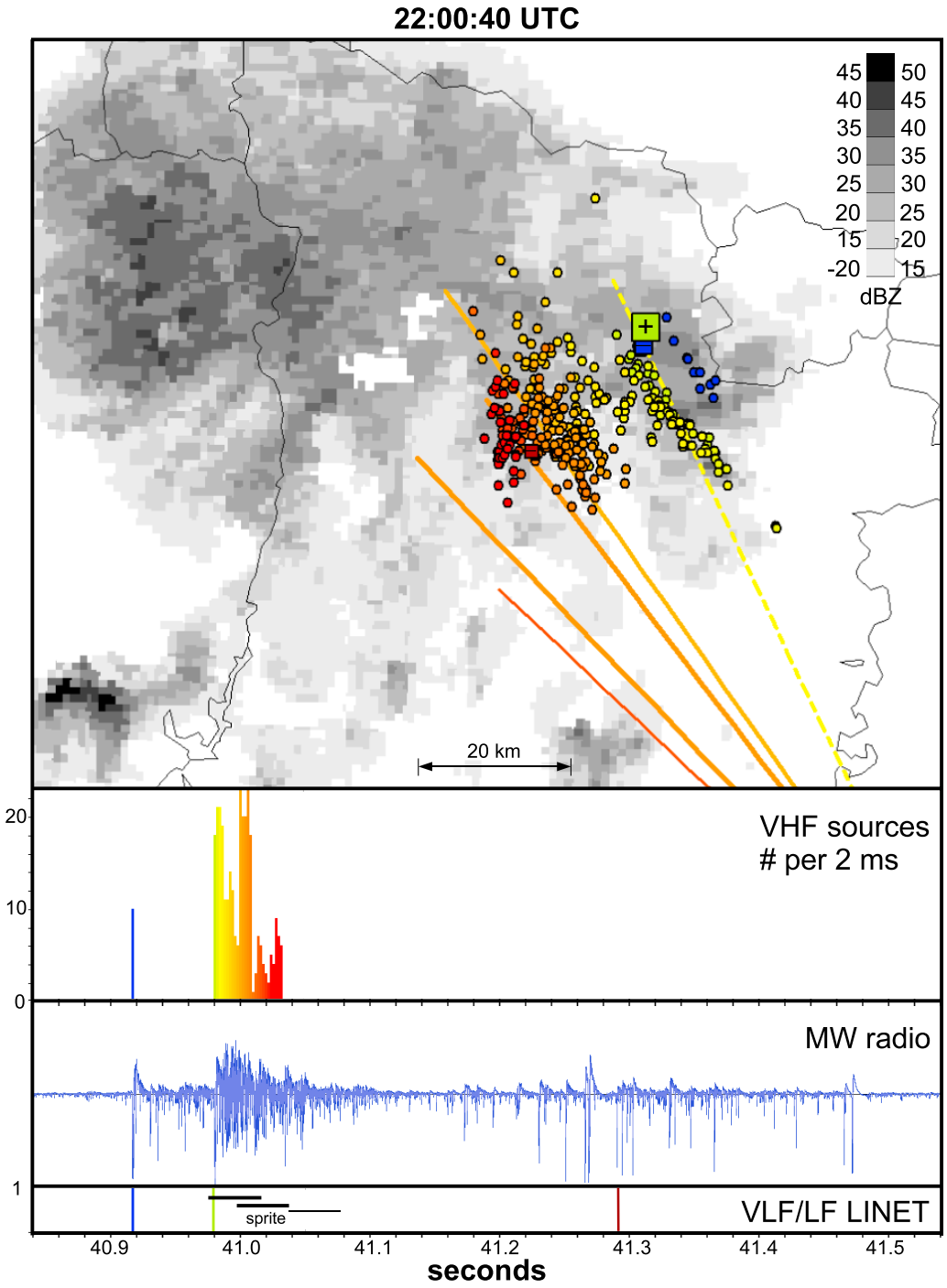

Figure 5. Spatiotemporal representation of detected lightning sources and sprites for the event of 2200:40 UTC. The background is the radar reflectivity image of 2200 UTC. The time evolution of XDDE VHF sources (circles) and LINET +CG and −CG (+ and − squares) are indicated by symbol color according to the lower images, with a resolution of 2 ms. Square size scales with peak current (see section 5.3 for details). Lines indicate the great circle paths from the camera to the sprite features marked in Figure 2c. The line ends correspond to an assumed sprite feature altitude of 83–87 km. The rightmost sprite azimuth has been drawn with a hatched line, since it is possible that more elements occurred outside view. The medium wave radio sferic shows the continuity of the lightning flash as a reference. The period covered by this graph spans 0.7 sec with ticks spaced every 20 ms.

Table 2. Characteristics of XDDE-Detected Sequences During the Period 2030–2230 UTC Grouped by the Peak Current of the Most Intense Stroke as Detected by LINET[a]

	Number of sequences in each category								
		Positive (kA)			Negative (kA)				
Sources	Sprite	0–10	10–25	>25	0–10	10–25	>25	IC	CG
dt = 300 ms									
< = 6	2	76	16	16	52	29	4	790	182
>6	15	110	33	18	64	32	10	203	233
>6 (%)	88%	59%	67%	53%	55%	52%	71%	20%	56%
dt = 700 ms:									
< = 6	2	58	11	12	41	21	3	522	136
>6	15	133	40	21	72	42	10	170	267
>6 (%)	88%	69%	78%	64%	64%	67%	77%	25%	66%

[a]The sequences in the sprite category are unique (i.e., do not occur in the peak current classes), whereas a sequence producing both positive and negative CG strokes occurs in the category according to the highest positive and negative polarity of these strokes.

fluctuations and their corresponding locations appear to coincide with the development of new sprites progressively to the southwest. It has to be noted that the complex second part of the sprite developed more to the southwest than the simultaneously detected activity, and also the following smaller columniform elements to the left of it. In this respect, there is a resemblance to the example of 21:09:10 UTC.

[29] The distances of the two parts of the sprite are not inconsistent with the corresponding lightning pattern in time. The altitude of the sprite, when considered to occur directly over the detected lightning path, is 72 km for the curtain-like feature at the right side and 76 km for the complex feature at the left side. This appears somewhat low. If we consider 82 km and 86 km instead (10 km higher), the sprite should have occurred between 5 and 10 km farther away than the edge of the detected lightning pattern, which is plausible. If a sprite were to surround the extensive lightning channels, as suggested by the observations of *Stanley* [2000], then closer sprite elements may have occurred as well which would have been out of the view of the camera (too high elevation angle) if they were closer than 60 km from the camera, assuming the lower part of such element reaching 60 km at 45° in the top of the image. This would imply a distance >20 km from the discharge edge nearest to the camera, which is not likely. However, a smaller element at greater altitude may have been missed even if closer to the detected VHF cluster location.

[30] The VHF cluster producing the sprite occurred in weak reflectivity, 20–35 dBZ, and no activity was detected in the region of moderate intensities to the west that produced the lightning activity for most of the earlier sprites, which seems related to the disappearance of the convective cells at the leading edge of the stratiform region. The rightmost extension of the sprite is not known (out of view), but the total visible width, assuming the distance of the sprite to be that of the underlying discharge, was 33 km. The leftmost extension was ~37 km from the center of the detected cluster. The orientation of the complex western part of the sprite is along the vertical, suggesting the triggering discharge must have been directly below the sprite, but it was not detected. Additional clues that detection was incomplete are the short total duration of the flash compared with those of the earlier events, and the much longer lasting sferic activity in the simultaneous long/medium wave radio recording which lasted certainly >500 ms after the triggering +CG. A −6 kA −CG or intracloud flash was detected after the end of the detected in-cloud activity at 41.292 sec near the southwestern tip of the discharge, without any subsequent detections.

6. Characteristics of Lightning Sequences Associated With Sprites Compared With Other Sequences

[31] The example events confirmed that the in-cloud lightning processes associated with sprite-producing +CG flashes are large and long lasting. Another characteristic is the occurrence of large bursts of VHF sources between +CG and sprites. This study would not be complete without answering the question how unique such properties are among other lightning flashes in the storm.

6.1. Procedure

[32] The basic procedure is summarized as follows:

[33] 1. Apply a moving average filter with a window of six to all sources (location).

[34] 2. Group raw data into "sequences" with intersource time interval less than threshold (300 ms).

[35] 3. Remove the first five moving-averaged sources of each sequence.

[36] 4. Calculate geometric properties of the sequences (needs two or more "averaged sources"; in other words, seven or more raw sources, except for the metrics "total number of sources" and "sequence duration").

[37] 5. Associate sequences to detected CG flashes and sprites and divide into categories.

[38] 6. Calculate statistics of geometric properties of sequences for each category.

[39] The moving average processing and their effects (step 1) and grouping XDDE data into "sequences" (step 2) were explained in detail earlier. Step 3 ensures that all moving-averaged sources belong indeed to the same sequence (does not include interpolation in space between separate sequences). The time interval used for the analysis was 2030–2230 UT, excluding the most active period of the storm to reduce the number of undesired combinations of independent flashes into one sequence. Geometric properties were calculated for each sequence, and the XDDE sequences were then associated to the data of LINET and classified by the highest peak current positive and negative CG occurring during a XDDE sequence. So, even if several CGs occurred during a sequence, for example, 51 kA, 23 kA, −7 kA, and −12 kA, the sequence was included in the highest peak current CG categories (e.g. >25 kA and −10 to −25 kA). The same sequence was excluded from the lower peak current CG categories (10–25 kA and 0 to −10 kA in this example). If a sequence contained a sprite, it was not included in any other category. XDDE sequences during which there was no LINET detection were listed as "IC" (intracloud), and the union of all sequences containing CG sequences of any polarity, including those associated with sprites, represents the "CG" category.

Table 3. Number of Sources

	Positive (kA)				Negative (kA)				
	Sprite	0–10	10–25	>25	0–10	10–25	>25	IC	CG
Median	63	8	10	7	7.5	8	13.5	3	8
95% CI Mean	43–128	11–17	13–31	10–25	13–22	10–25	6.1–34	4.2–4.9	14–20
St.Dev	82	19	31	31	24	29	24	5.5	30

[40] Tables 2–7 show a summary of characteristics by sequence category (sprite, +CG of 0–10, 10–25, >25 kA, −CG of 0–10, 10–25, >25 kA, IC, and all CG: all CGs combined). The absolute values of the metrics in Tables 2–7 depend on the performance of the XDDE system, the distance of the lightning to the sensors, and the selected sequence time criterion (*dt*), but nevertheless there are significant differences between some of the categories. The choice of moving average window size affects all sequences equally (uniformly) and cannot cause shifts between categories. The time criterion can cause similar shifts as the moving average in our tests, which appear to be rather small, but these shifts may not be uniform across the different categories. Whenever the statistical significance of differences between categories appears to be marginal (<99% or small overlap between confidence intervals), a double check was done with dt = 700 ms.

6.2. Category Population Size

[41] The number of sequences in each category is displayed in Table 2. The top row indicates the number of sequences that had six or fewer sources, which are excluded from the statistics which required the moving average. In particular, the category of −CG sequences with a peak current of 25 kA or higher is small (only 10 sequences) and will probably not yield reliable statistics. The sprite category contains 17 sequences, 15 of them large enough to calculate geometric properties. While this is a small number as well, the statistics show this category to be consistently different from the other classes.

[42] Table 2 also lists the percentage of sequences with more than six sources of the total detected for that category. Here, on average, ~56% of CG sequences without sprites were large enough to be considered for the statistics involving the moving average. For sprites this was 88%, and for intracloud sequences only 20%, which indicates that XDDE typically displays just a few sources for the majority of IC sequences. Note that the cases with a total absence of sources are not displayed.

[43] To get an idea how large the influence is of the chosen sequence criterion (*dt*) on the number of sequences, the numbers have been calculated both for dt = 300 ms and dt = 700 ms. For most categories, the absolute number of sequences greater than six sources increases by some 15%–20% when increasing *dt*, with the exception being the category of IC sequences (−16%), of which the sources apparently become part of a sequence containing CG flashes. Listed *P* values (two-tailed) were obtained using the nonparametric Mann-Whitney (Wilcoxon) statistical significance test, also known as the rank sum test, while 95% confidence intervals for the mean assumed a Student's *t*-distribution.

6.3. Number of Sources Per Sequence

[44] This simple statistic includes all sequences with one or more sources (Table 3). The median value for all CG-containing sequences (rightmost column) is eight sources. IC sequences are much smaller with a median of three sources and a six times smaller standard deviation. This difference is extremely statistically significant (P = 0). Sequences with sprites contain a remarkably high number of sources (median of 63), even when compared with sequences that contain one or more +CG strokes. The median is about seven times higher than for other +CG categories. This difference is extremely statistically significant (P = 0.0000206). Using an alternative *dt* of 700 ms, the medians increase by three sources for most CG categories while the standard deviations stay the same.

6.4. Linear Dimensions

[45] We calculated the maxima and minima of moving-averaged source locations for latitude and longitude, marking a bounding box of the sequence. The diagonal of this box (Table 4) is the largest diameter the sequence could have been. Sprite-producing sequences are the largest horizontally extended sequences with medians more than twice the median for all CG: 43 km versus 17 km. The difference between sprite and +CG 10–25 kA categories is statistically significant (P = 0.00152), but between sprite and +CG >25 kA is not significant (P = 0.148, P = 0.056 for dt = 700 ms). This does not imply that the nonsprite sequences cannot be large. The 95th percentile value for the combined CG category is 68 km, for IC 34 km, and for sprite-associated sequences 86 km. The maximum size is constrained by the size of the stratiform precipitation area. No significant differences are found between the +CG and −CG group and peak currents. Note that this metric is rather sensitive to *dt* with all values increasing by 2–4 km for dt = 700 ms, the largest difference is the median for +CG 10–25 kA going from 12 to 24 km, and the sprite category median, which increases to 57 km.

Table 4. Diagonal of Bounding Latitude-Longitude Box (km)

	Positive (kA)				Negative (kA)				
	Sprite	0–10	10–25	>25	0–10	10–25	>25	IC	CG
Median	43	18	12	30	19	20	15	9.5	17
95% CI Mean	35–59	19–26	15–32	19–46	22–33	16–31	7.5–32	11–13	21–26
St.Dev	22	18	24	28	22	22	17	10	21

Table 5. Dimension Perpendicular to the Convective Line (km)

	Positive (kA)				Negative (kA)				
	Sprite	0–10	10–25	>25	0–10	10–25	>25	IC	CG
Median	37	8.5	8.1	11	9.4	8.2	11	4.5	7.9
95% CI Mean	26–44	9.0–13	7.1–21	7.2–23	11–16	6.4–19	3.6–21	5.6–7.3	11–14
St.Dev	16	9.4	19	16	11	18	13	6.1	14

[46] Note also the interesting fact that the IC category differs statistically very significantly from sequences associated with low peak current positive and negative CG flashes, as detected by LINET, not only in size but also in number of sources (IC are twice as small).

6.5. Line Perpendicular Dimension

[47] The thunderstorm convective line was oriented approximately along a 150° (or −30°) angle with the meridians. Sprite sequences propagated under a median angle of 65° to the line, compared with 28° for the category of all CGs (data not shown). This was determined from the difference in location of the beginning of a sequence and the averaged (central) location of the sequence. Since virtually all sprite-producing sequences started at the convective line, it is more interesting to compare the size of the sequence in the direction perpendicular to the convective line, best reflecting the convective-to-stratiform distance of propagation. To do this, a simple rotation of the coordinate system was performed after converting latitude and longitude to a kilometer-based grid. The y-axis was taken as the direction perpendicular to the line. Table 5 shows the result ($y_{max} - y_{min}$ per sequence). It is immediately apparent that the sprite category of sequences has indeed the largest dimension perpendicular to the line with a median of 37 km (maximum 56 km). The all-CG category has a median of only 8 km, so the difference is more pronounced than for the box diagonal. While the medians of the >25 kA categories are slightly larger (11 km) than for weaker CG categories, the differences are by far not statistically significant, as is already obvious from the confidence intervals.

6.6. Duration

[48] Table 6 shows the duration computed as the time between the first and the last source of the sequence. Table 7 shows the interquartile range (IQR) of VHF source times per sequence, "IQR-time," as an alternative representation: the time interval in which 50% of the sources of the sequence occurred. Sequences with six or fewer sources are included as well. Keeping in mind the criterion that defines a sequence (300 ms maximum interval) and the imperfect detection efficiency, the sequences in the IC category clearly last the shortest with a median of 84 ms, whereas the sequences of the CG category last almost four times as long with 302 ms and the sequences with sprites last the longest with a median of 539 ms. The longest lasting sprite-associated sequence had a duration of 2.7 sec, and the longest nonsprite CG sequence lasted 1.7 sec (95th percentile of 1.3 sec). IC sequences lasted up to 989 ms (95th percentile of 564 ms).

[49] However, the differences in duration between the sprite category and +CG categories are not significant at the 95% level ($P = 0.19$). For $dt = 700$ ms, median durations increased by a factor of 2 to 3 for all categories, but significance remained low ($P = 0.07$). Apparently, this is due to the large standard deviation within the sprite category, which is twice as large as the value for all CG combined (782 ms versus 386 ms).

[50] Although not immediately obvious from Tables 6 and 7, the difference between positive and negative CG sequences with peak current >10 kA (241 and 450 ms median durations and 61 and 150 ms median IQR-time, respectively, are statistically significant at the 95% level ($P = 0.011$; $P = 0.021$)). At $dt = 700$ ms, the differences become totally insignificant, mainly due to the much larger increase for +CG-containing sequences. The multistroked behavior of −CG flashes appears responsible for the difference at <300 ms time scales [see *Valine and Krider*, 2002].

7. Conclusions and Discussion

[51] This study considered the in-cloud lightning component associated with the lightning flashes of a small leading line trailing stratiform thunderstorm system that produced 17 detected sprites.

7.1. Spatial and Temporal Dimensions of Sprite-Producing Flashes

[52] Sprite-triggering discharges emitted on average (median) seven times more VHF sources, detected by the interferometer system in northeastern Spain, lasted longer, and were horizontally twice as extensive as the average CG sequence, in particular in the direction perpendicular to the linear convective region (four times as extensive). The variation in duration of sequences was rather large and overlapping for most CG categories. Sprite-associated sequences and negative CG sequences tended to have twice as long median durations as sequences with positive CGs (>10 kA). Intracloud sequences were the smallest, on

Table 6. Sequence Duration (ms)

	Positive (kA)				Negative (kA)				
	Sprite	0–10	10–25	>25	0–10	10–25	>25	IC	CG
Median	539	336	238	244	396	414	512	84	302
95% CI Mean	308–1112	377–477	264–503	186–542	383–543	366–588	337–842	136–164	371–450
St.Dev	782	334	398	468	407	385	397	189	386

Table 7. Sequence Duration (IQR of Source Times) (ms)

	Positive (kA)				Negative (kA)				
	Sprite	0–10	10–25	>25	0–10	10–25	>25	IC	CG
Median	115	111	59	79	142	167	159	68	109
95% CI Mean	83–492	136–188	80–195	65–232	151–227	138–241	98–327	87–116	147–191
St.Dev	369	137	162	167	152	143	160	107	171

average about half the size and duration of CG sequences. The median horizontal size of sprite-producing sequences was 43 km, with a median propagation distance of 37 km perpendicular to the convective line, where the discharges usually initiated. Convective-to-stratiform lightning propagation has also been reported with time of arrival lightning mapping systems by *Lang et al.* [2004], *Carey et al.* [2005], and *Ely et al.* [2008]. This appears to be the first time that discharges of this remarkable size are documented in Europe. In the United States, such observations date back to 1956 [*Ligda*, 1956] and have become known as "spider lightning" [*Mazur et al.*, 1998]. Note that the term *spider lightning* is usually applied to large horizontal lightning channels under the base of the cloud which are visible to an observer on the ground. In case of horizontally extensive flashes detected by a mapping system these may also occur inside the cloud, hidden from view. The flashes producing sprites in our storm were of a similar size to those reported by *Lyons et al.* [2003], but half the size of the average horizontally extensive lightning flash in the MCS studied by *Lang et al.* [2004].

7.2. Characteristics of Detection of Sprite-Associated Lightning by the XDDE Interferometer System

[53] Comparison of VHF sources with sferics as in the examples shown reveals that the XDDE system does not detect lightning processes continuously, as a VHF time of arrival lighning mapping array would, but instead shows intermittent VHF pulses. The XDDE bursts tended to be correlated with the stronger sferics instead of the weaker periods of sferics. An important finding is that +CGs, particularly those that trigger sprites, do initiate bursts of many VHF sources, which apparently are associated with the discharging process supplying a continuing current to the grounded channel [*van der Velde et al.*, 2006]. The system is apparently most sensitive to this particular form of lightning process. The bursts are the major contributor to the larger total number of sources for sprite sequences compared with other sequences in the statistical results. The duration of such bursts tended to be short, generally 2–10 ms, but was longer for the sprite-producing flashes that occurred closer to the detection system. Compared with data from a French SAFIR interferometer system analyzed by *van der Velde et al.* [2006], the later-generation (LS8000/CP8000) XDDE interferometer system showed many more VHF sources during the period between the +CG stroke and the sprite, although it is likely that a significant part of the post-+CG activity is still not located by the central processor due to the spatiotemporal complexity of the discharge with many simultaneous processes [*Mazur et al.*, 1997, 1998]. *Mazur et al.* [1997] showed that it is characteristic for an interferometric system such as the XDDE (SAFIR) to miss a large part of the negative leader activity, compared to short baseline time-of-arrival systems, which record leader activity continuously. Positive leaders are even more difficult to detect, also for time-of-arrival systems, because their radio emissions are much weaker [*Shao and Krehbiel*, 1996, p. 26,663; *Shao et al.*, 1999].

[54] In a number of cases, the XDDE system detected a second (sometimes first), usually less intense burst of sources after some delay to the +CG, which corresponded with a long-delayed carrot sprite in space and time. In this study, this was the only demonstrable difference between detected sequences producing carrots (which tend to be delayed longer compared to columns [*van der Velde et al.*, 2006]) and those producing other types of sprites, which were mostly groups of weak but closely spaced "grassy"-looking elements. It is possible that the secondary burst was produced by a missed +CG, or instead by enhanced in-cloud activity leading to an M-component (current maximum) during the continuing current stage of the +CG flash as documented by high-speed video measurements of natural +CG flashes by *Campos et al.* [2009] and by remote ELF/VLF radio measurements of lightning flashes associated with long-delayed sprites by *Li et al.* [2008]. The bursts explain well why a long-delayed sprite occurred, but not all bursts were associated with detected +CG flashes or sprites, an example of which was shown (2124:40 UT event). The possibility exists that secondary bursts after +CGs are a result of a short blackout in the detection of a continuous cluster of VHF sources and that their detection was resumed if the activity continued for long enough (which can be reason in itself to produce a delayed sprite).

7.3. Storm-Relative Location of Leading In-Cloud Activity and +CG Strokes in Sprite-Producing Flashes

[55] The typical sprite-producing lightning discharge as detected by the XDDE system showed relatively little leading (pre-CG) in-cloud activity, in part due to failure to detect leaders. Pre-+CG VHF sources were absent in 8 of the 17 sprite cases and started in or close to the convective region in the remaining 9 sprite cases. In this storm system, +CG discharges that triggered sprites were often (11 of 17 cases) located at the rear side of a convective core, sometimes followed by another +CG striking deeper inside the stratiform precipitation area which may trigger a second sprite. In other cases, leading in-cloud activity started inside the convective region, and the first +CG struck well inside the stratiform region. These occurred mainly between 2117–2146, when the stratiform region was largest and the transition zone of lower reflectivity behind the convection was most pronounced. Our observations are in line with those of *Lang et al.* [2004], who also found comparatively few +CG flashes (9 of 39) which originated inside the stratiform region.

[56] In 9 of the 17 cases, VHF sources continued to be detected after the sprites in the center and southwest (rear) side of the stratiform region for several hundred milliseconds. During this period, detections of low peak current (~6 kA) of predominantly negative polarity were indicated by LINET. In a few cases such as 2109 (example 1), 2111, and 2115, a strong (>60 kA) or long multiple-stroked (10–13 strokes) deep stratiform −CG occurred during the late stages of the sequence. It is possible that these discharges, tapping stratiform negative charge layers, occur in response to enhanced electric fields between cloud and ground after the removal of large amounts of positive charge which caused the sprite. LINET often showed more detections than EUCLID during the part of the sequences after the sprites, and the XDDE showed VHF sources close to these CG. Simultaneous audio records of medium wave radio sferics (in Figures 3–5) also show these CGs (or strong in-cloud lightning) to be part of ongoing sferic activity. *Soula et al.* [2009, 2010], using *Météorage* (EUCLID) lightning detection data, documented similar sequences of +CG and −CG flashes throughout the stratiform region close to the times of sprites.

[57] Not only did sprite-associated VHF sequences start at the convective region, such as those reported by *Lang et al.* [2004], *Carey et al.* [2005], and *Ely et al.* [2008], but we also observed that the temporal and spatial occurrence of sprite-producing discharges followed the cycles of convective cores, generators of charge, in the MCS. The flashes showed a preference for the developing stage of these cores from which they originated (Table 1). It has to be noted that this occurred during the larger-scale decay of sections of the convective region. Additionally, we observed that despite there being a large, moderate reflectivity stratiform precipitation area still present after 2150 UTC, no sprites were triggered over this section after core C disappeared, the last core adjacent to this area. In fact, the sprite-producing discharges of 2156, 2200, and 2203 UTC occurred in a weaker and narrower part of stratiform rain, triggered from core E at the east side of the cell (as in Figure 5). A related observation is that of *Shafer et al.* [2000], who noted that CG lightning flash rates in convective and stratiform regions of an MCS exhibited simultaneous trends, suggesting a close link. A pronounced isolated "sprite +CG producing convective cell" also occurred in the parallel stratiform MCS on 28–29 August 2003 over France during EuroSprite (using MCS morphological definitions of *Parker and Johnson* [2000]). So, it can be concluded that the presence of a convective cell is beneficial for triggering of horizontally extensive sprite-producing lightning flashes.

[58] There could be several reasons for the connection between sprite-producing discharges and active convective cores. First, the discharge needs a strong local electric field for its initiation, which may be most easily attained in a growing or mature convective cell of the storm. Second, the discharge (if not triggered from a ground-based object, e.g., *Rakov and Uman* [2003], chapter 6) most likely develops in a bidirectional way (zero net charge, equipotential channel [*Mazur and Ruhnke*, 1993, 1998]) with a positive leader branch and a negative leader branch, each propagating into pockets of opposite charge in the storm (potential wells, *Coleman et al.* [2003]). This implies that besides the negative leader finding its way into the stratiform positive charge layer, the positive leader needs an equal body of negative charge for the entire flash to expand to large dimensions. This negative charge may be most easily accessed in the convective region itself. Furthermore, charge is consumed in the process, so that rapid regeneration of charge, both positive and negative, is necessary to reproduce large discharges with reasonable frequency. This is most probable in updraft regions, and indeed the observation that sprite-associated sequences occur during the growing and mature stage of convective cells points to this requirement.

[59] Also, the placement of +CG strokes inside or not far from the convective region may be explained by the bidirectional development of lightning discharges in light of what happens when positive and negative charges are not in balance [*Krehbiel et al.*, 2008]. An imbalance may be assumed because the stratiform positive charge reservoir is usually a vertically narrow layer (<1 km) of very large horizontal dimensions, several tens of kilometers wide, containing charge densities about equal to those found in convective cells (e.g., 2–4 nC m^{-3} [*Hunter et al.*, 1992; *Marshall and Rust*, 1993]). On the other hand, charge in the convective cells is typically found over a depth of 1–3 km, but having smaller horizontal dimensions (usually <10 km as can also be assumed to be the case in this storm, based on the area with radar reflectivity >40 dBZ). So, when a large, contiguous negative convective charge region is lacking, an imbalance exists between positive and negative charge for discharges that can tap into both reservoirs. During bidirectional development, the positive leaders can then consume most of the negative charge and subsequently grow to ground in the vicinity of the convective core forming a +CG while the negative leaders encounter a sufficiently high potential gradient in their surroundings to keep expanding deeper into stratiform positive charge. This is analogous to the concept exploited by *Krehbiel et al.* [2008] to explain the escape of lightning discharges from a cloud in the form of CG flashes, bolts from the blue, cloud to air discharges, and even gigantic jets, which is supported by their modeling results.

[60] For the majority of our sprite-associated discharges, VHF activity was detected only in and near the convective region and after a +CG occurred, so negative leaders venturing deep into the stratiform region before the +CG were not detected. As soon as a +CG connection to ground occurs, the conductive ground becomes the supplier of opposite charge, allowing negative leaders to discharge an extensive layer of positive charge more effectively than by virgin bileader breakdown. Examples from the STEPS 2000 campaign, shown by *Lyons et al.* [2006] and *Marshall et al.* [2007], using a time-of-arrival lightning mapping array, which is more sensitive to individual pulses emitted by leaders than the XDDE system, also demonstrated a single uniform expansion of lightning channels after the +CG stroke in a dendritic fashion.

[61] A consequence of the bidirectional nature of propagation could be that when the amount of accessible negative charge is larger, the longer it may take until the +CG occurs (after its consumption), the deeper the initial negative leader branch can enter into the stratiform region, and the more effective charge removal following a +CG could proceed,

starting from a more developed initial set of negative leader branches.

7.4. Positioning and Size of Sprites Relative to the In-Cloud Lightning Component

[62] An important conclusion is that in case of sprites displaced from the +CG by tens of kilometers (including the examples in Figure 3 and 4), the sprite azimuth occurred over VHF sources occurring after the +CG. In other cases, such as the case presented in Figure 5, the horizontal sprite size and direction of development matched well with the size and development of the in-cloud lightning underneath. So, it confirms the location of in-cloud discharge processes as the main factor of sprite positioning, at least the larger structure. The obvious reason is that the branches in the cloud gather charge and supply it as a continuing current to the grounded +CG channel [e.g., *Lyons et al.*, 2003; *van der Velde et al.*, 2006; *Marshall et al.*, 2007], so this must also be the location above which the largest quasi-electrostatic field due to the charge moment change is felt.

[63] Note that for a few of the sprite-producing discharges, such as examples 1 and 3, sprites also occurred laterally displaced from the simultaneously detected in-cloud discharge activity. This is most probably the result of the system's failure to detect a part of the lightning discharge. However, *Stanley* [2000] noted that the elements of grouped sprites appeared to occur at the perimeter of the associated mapped lightning flashes, not directly above the largest charge removal. This is a topic that deserves more attention and requires multistation simultaneous observations to pinpoint the sprite element locations, as well as high time resolution to compare to lightning development.

[64] Large stratiform lightning flashes are very complex, and more research is necessary to explain their full behavior with respect to bidirectional development, the role of convective cores in their initiation, positive and negative charge layers and internal irregularities, and different types of associated ground strokes, including those that initiate from tall structures at the ground or from mountains.

[65] **Acknowledgments.** This study was conducted with the support of the Spanish Ministry of Science and Innovation under grant ESP2007-66542-C04-02.

[66] Z. Pu thanks the reviewers for their assistance in evaluating this paper.

References

Barrington-Leigh, C. P., U. S. Inan, M. Stanley, and S. A. Cummer (1999), Sprites triggered by negative lightning discharges, *Geophys. Res. Lett.*, *26*(24), 3605–3608, doi:10.1029/1999GL010692.

Bell, T. F., S. C. Reising, and U. S. Inan (1998), Intense continuing currents following positive cloud-to-ground lightning associated with red sprites, *Geophys. Res. Lett.*, *25*(8), 1285–1288, doi:10.1029/98GL00734.

Betz, H.-D., K. Schmidt, P. Oettinger, and M. Wirz (2004), Lightning detection with 3-D discrimination of intracloud and cloud-to-ground discharges, *Geophys. Res. Lett.*, *31*, L11108, doi:10.1029/2004GL019821.

Boccippio, D. J., E. R. Williams, S. J. Heckman, W. A. Lyons, I. T. Baker, and R. Boldi (1995), Sprites, ELF transients, and positive ground strokes, *Science*, *269*, 1088–1091.

Campos, L. Z. S., M. M. F. Saba, O. Pinto Jr., and M. G. Ballarotti (2009), Waveshapes of continuing currents and properties of M-components in natural positive cloud-to-ground lightning, *Atmos. Res.*, *91*, 416–424, doi:10.1016/j.atmosres.2008.02.020.

Carey, L. D., M. J. Murphy, T. L. McCormick, and N. W. S. Demetriades (2005), Lightning location relative to storm structure in a leading-line, trailing-stratiform mesoscale convective system, *J. Geophys. Res.*, *110*, D03105, doi:10.1029/2003JD004371.

Cho, M., and M. J. Rycroft (2001), Non-uniform ionisation of the upper atmosphere due to the electromagnetic pulse from a horizontal lightning discharge, *J. Atmos. Solar-Terr. Phys.*, *63*, 559–580.

Coleman, L. M., T. C. Marshall, M. Stolzenburg, T. Hamlin, P. R. Krehbiel, W. Rison, and R. J. Thomas (2003), Effects of charge and electrostatic potential on lightning propagation, *J. Geophys. Res.*, *108*(D9), 4298, doi:10.1029/2002JD002718.

Cummer, S., and M. Füllekrug (2001), Unusually intense continuing current in lightning produces delayed mesospheric breakdown, *Geophys. Res. Lett.*, *28*(3), 495–498, doi:10.1029/2000GL012214.

Cummer, S. A., and W. A. Lyons (2005), Implications of lightning charge moment changes for sprite initiation, *J. Geophys. Res.*, *110*, A04304, doi:10.1029/2004JA010812.

Cummer, S. A., N. Jaugey, J. Li, W. A. Lyons, T. E. Nelson, and E. A. Gerken (2006), Submillisecond imaging of sprite development and structure, *Geophys. Res. Lett.*, *33*, L04104, doi:10.1029/2005GL024969.

Ely, B. L., R. E. Orville, L. D. Carey, and C. L. Hodapp (2008), Evolution of the total lightning structure in a leading-line, trailing-stratiform mesoscale convective system over Houston, Texas, *J. Geophys. Res.*, *113*, D08114, doi:10.1029/2007JD008445.

Füllekrug, M., M. Ignaccolo, and A. Kuvshinov (2006), Stratospheric Joule heating by lightning continuing current inferred from radio remote sensing, *Radio Sci.*, *41*, RS2S19, doi:10.1029/2006RS003472.

Franz, R. C., R. J. Nemzek, and J. R. Winckler (1990): Television image of a large upward electrical discharge above a thunderstorm system, *Science*, *249*, 48–51.

Greenberg, E., C. Price, Y. Yair, M. Ganot, J. Bor, and G. Satori (2007), ELF transients associated with sprites and elves in eastern Mediterranean winter thunderstorms, *J. Atmos. Solar-Terr. Phys.*, *69*(13), 1569–1586.

Greenberg, E., C. Price, Y. Yair, O. Chanrion, and T. Neubert (2009), ELF/VLF signatures of sprite-producing lightning discharges observed during the 2005 EuroSprite campaign, *J. Atmos. Solar-Terr. Phys.*, *71*(12), 1254–1266, doi:10.1016/j.jastp.2009.05.005.

Hu, W., S. Cummer, W. A. Lyons, and T. Nelson (2002), Lightning charge moment changes for the initiation of sprites, *Geophys. Res. Lett.*, *29*(8), 1279, doi:10.1029/2001GL014593.

Hu, W., S. A. Cummer, and W. A. Lyons (2007), Testing sprite initiation theory using lightning measurements and modeled electromagnetic fields, *J. Geophys. Res.*, *112*, D13115, doi:10.1029/2006JD007939.

Huang, E., E. Williams, R. Boldi, S. Heckman, W. Lyons, M. Taylor, T. Nelson, and C. Wong (1999), Criteria for sprites and elves based on Schumann resonance observations, *J. Geophys. Res.*, *104*(D14), 16,943–16,964, doi:10.1029/1999JD900139.

Hunter, S. M., T. J. Schuur, T. C. Marshall, and W. D. Rust, (1992): Electric and kinematic structure of the Oklahoma mesoscale convective systems of 7 June 1989, *Mon. Weather Rev.*, *120*, 2226–2239.

Kasemir, H. (1960), A contribution to the electrostatic theory of a lightning discharge, *J. Geophys. Res.*, *65*(7), 1873–1878, doi:10.1029/JZ065i007p01873.

Kong, X., X. Qie, and Y. Zhao (2008), Characteristics of downward leader in a positive cloud-to-ground lightning flash observed by high-speed video camera and electric field changes, *Geophys. Res. Lett.*, *35*, L05816, doi:10.1029/2007GL032764.

Krehbiel, P. R., J. A. Riousset, V. P. Pasko, R. J. Thomas, W. Rison, M. A. Stanley, and H. E. Edens (2008), Upward electrical discharges from thunderstorms, *Nat. Geosci.*, *1*(4), 233–237, doi:10.1038/ngeo162.

Lang, T. J., S. A. Rutledge, and K. C. Wiens (2004), Origins of positive cloud-to-ground lightning flashes in the stratiform region of a mesoscale convective system, *Geophys. Res. Lett.*, *31*, L10105, doi:10.1029/2004GL019823.

Li, J., S. A. Cummer, W. A. Lyons, and T. E. Nelson (2008), Coordinated analysis of delayed sprites with high-speed images and remote electromagnetic fields, *J. Geophys. Res.*, *113*, D20206, doi:10.1029/2008JD010008.

Ligda, M. G. H., (1956), The radar observations of lightning, *J. Atmos. Terr. Phys.*, *9*, 329–346. doi:10.1016/0021-9169(56)90152-0.

Lyons, W. A. (1996), Sprite observations above the U.S. High Plains in relation to their parent thunderstorm systems, *J. Geophys. Res.*, *101*(D23), 29,641–29,652, doi:10.1029/96JD01866.

Lyons, W. A., T. E. Nelson, E. R. Williams, S. A. Cummer, and M. A. Stanley (2003), Characteristics of sprite-producing positive cloud-to-ground lightning during the 19 July 2000 STEPS mesoscale convective systems, *Mon. Weather Rev.*, *131*(10), 2417–2427.

Lyons, W. A., L. M. Andersen, T. E. Nelson, and G. R. Huffines (2006), Characteristics of sprite-producing electrical storms in the STEPS 2000

domain. Online summary and CD, 2nd Conf. on Meteorological Applications of Lightning Data, American Meteorological Society, Atlanta, GA, USA, 19 pp.

MacGorman, D. R., and W. D. Rust (1998), *The Electrical Nature of Storms*, pp. 258–286, Oxford University Press, New York.

Marshall, R. A., U. S. Inan, and W. A. Lyons (2007), Very low frequency sferic bursts, sprites, and their association with lightning activity, *J. Geophys. Res.*, *112*, D22105, doi:10.1029/2007JD008857.

Marshall, T. C., and W. D. Rust (1993), Two types of vertical electrical structures in stratiform precipitation regions of mesoscale convective systems, *Bull. Am. Meteorol. Soc.*, *74*, 2159–2170.

Matsudo, Y., T. Suzuki, K. Michimoto, K. Myokei, and M. Hayakawa (2009), Comparison of time delays of sprites induced by winter lightning flashes in the Japan Sea with those in the Pacific Ocean, *J. Atmos. Sol. Terr. Phys.*, *71*, 101–111, doi:10.1016/j.jastp.2008.09.040.

Mazur, V. (2002), Physical processes during development of lightning flashes, *Comptes Rendus Phys.*, *3*, 1393–1409.

Mazur, V., and L. Ruhnke (1993), Common physical processes in natural and artificially triggered lightning, *J. Geophys. Res.*, *98*(D7), 12,913–12,930, doi:10.1029/93JD00626.

Mazur, V., and L. Ruhnke (1998), Model of electric charges in thunderstorms and associated lightning, *J. Geophys. Res.*, *103*(D18), 23,299–23,308, doi:10.1029/98JD02120.

Mazur, V., E. Williams, R. Boldi, L. Maier, and D. E. Proctor (1997), Initial comparison of lightning mapping with operational time-of-arrival and interferometric systems, *J. Geophys. Res.*, *102*(D10), 11,071–11,086, doi:10.1029/97JD00174.

Mazur, V., X. Shao, and P. R. Krehbiel (1998), "Spider" lightning in intracloud and positive cloud-to-ground flashes, *J. Geophys. Res.*, *103*(D16), 19,811–19,822, doi:10.1029/98JD02003.

McHarg, M. G., H. C. Stenbaek-Nielsen, and T. Kammae (2007), Observations of streamer formation in sprites, *Geophys. Res. Lett.*, *34*, L06804, doi:10.1029/2006GL027854.

Mika, Á., C. Haldoupis, R. A. Marshall, T. Neubert, and U. S. Inan (2005), Subionospheric VLF signatures and their association with sprites observed during EuroSprite-2003, *J. Atmos. Sol. Terr. Phys.*, *67*, 1580–1597, doi:10.1016/j.jastp.2005.08.011.

Montanyà, J., N. Pineda, V. March, A. Illa, D. Romero, and G. Solà (2006), Experimental evaluation of the Catalan Lightning Detection Network, paper presented at *19th International Lightning Detection Conference*, Tucson, AZ, USA.

Montanyà, J., O. van der Velde, D. Romero, V. March, G. Solà, N. Pineda, M. Arrayás, J. L. Trueba, V. Reglero, and S. Soula (2010), High-speed intensified video recordings of sprites and elves over the western Mediterranean Sea during winter thunderstorms, *J. Geophys. Res.*, *115*, A00E18, doi:10.1029/2009JA014508.

Morimoto, T., Z. Kawasaki, and T. Ushio (2005), Lightning observations and consideration of positive charge distribution inside thunderclouds using VHF broadband digital interferometry, *Atmos. Res.*, *76*, 445–454, doi:10.1016/j.atmosres.2004.11.024.

Moudry, D. R., H. C. Stenbaek-Nielsen, D. D. Sentman, and E. M. Wescott (2003), Imaging of elves, halos and sprite initiation at 1 ms time resolution, *J. Atmos. Sol. Terr. Phys.*, *65*, 509–518, doi:10.1016/S1364-6826(02)00323-1.

Neubert, T., et al. (2005), Co-ordinated observations of transient luminous events during the EuroSprite2003 campaign, *J. Atm. Sol.-Terr. Phys.*, *67*, 807–820, doi:10.1016/j.jastp.2005.02.004.

Neubert, T., et al. (2008), Recent results from studies of electric discharges in the mesosphere, *Surv. Geophys.*, *29*, 71–137, doi:10.1007/s10712-008-9043-1.

Ohkubo, A., H. Fukunishi, Y. Takahashi, and T. Adachi (2005), VLF/ELF sferic evidence for in-cloud discharge activity producing sprites, *Geophys. Res. Lett.*, *32*, L04812, doi:10.1029/2004GL021943.

Parker, M. D., and R. H. Johnson (2000), Organizational modes of midlatitude mesoscale convective systems, *Mon. Weather Rev.*, *128*, 3413–3436.

Pasko, V. P., U. S. Inan, and T. F. Bell (1996), Sprites as luminous columns of ionization produced by quasi-electrostatic thundercloud fields, *Geophys. Res. Lett.*, *23*(6), 649–652, doi:10.1029/96GL00473.

Pasko, V. P., U. S. Inan, and T. F. Bell (1997), Sprites as evidence of vertical gravity wave structures above mesoscale thunderstorms, *Geophys. Res. Lett.*, *24*(14), 1735–1738, doi:10.1029/97GL01607.

Pasko, V. P., U. S. Inan, and T. F. Bell (1998), Spatial structure of sprites, *Geophys. Res. Lett.*, *25*(12), 2123–2126, doi:10.1029/98GL01242.

Proctor, D., R. Uytenbogaardt, and B. Meredith (1988), VHF radio pictures of lightning flashes to ground, *J. Geophys. Res.*, *93*(D10), 12,683–12,727, doi:10.1029/JD093iD10p12683.

Rakov, V. A., and M. A. Uman (2003), *Lightning: Physics and Effects*, Cambridge Univ. Press, New York.

Rhodes, C., X. Shao, P. Krehbiel, R. Thomas, and C. Hayenga (1994), Observations of lightning phenomena using radio interferometry, *J. Geophys. Res.*, *99*(D6), 13,059–13,082, doi:10.1029/94JD00318.

Richard, P., and J. Y. Lojou (1996), Assessment of application of storm cell electrical activity monitoring to intense precipitation forecast, paper presented at 10th International Conference on Atmospheric Electricity, June 10–14, Osaka, Japan, pp. 284–287.

Richard, P., A. Delannoy, G. Labaune, and P. Laroche (1986), Results of spatial and temporal characterization of the VHF-UHF radiation of lightning, *J. Geophys. Res.*, *91*, 1248–1260, doi:10.1029/JD091iD01p01248.

Rust, W. D., D. R. MacGorman, and W. L. Taylor (1985), Photographic verification of continuing current in positive cloud-to-ground flashes, *J. Geophys. Res.*, *90*, 6144–6146, doi:10.1029/JD090iD04p06144.

Saba, M. M. F., M. G. Ballarotti, and O. Pinto Jr. (2006), Negative cloud-to-ground lightning properties from high-speed video observations, *J. Geophys. Res.*, *111*, D03101, doi:10.1029/2005JD006415.

Saba, M. M. F., K. L. Cummins, T. A. Warner, E. P. Krider, L. Z. S. Campos, M. G. Ballarotti, O. Pinto Jr., and S. A. Fleenor (2008), Positive leader characteristics from high-speed video observations, *Geophys. Res. Lett.*, *35*, L07802, doi:10.1029/2007GL033000.

São Sabbas, F. T., D. D. Sentman, E. M. Wescott, O. Pinto Jr., O. Mendes Jr., and M. J. Taylor (2003), Statistical analysis of space–time relationships between sprites and lightning, *J. Atmos. Sol.-Terr. Phys.*, *65*(5), 525–535.

Sentman, D. D., E. M. Wescott, D. L. Osborne, D. L. Hampton, and M. J. Heavner (1995), Preliminary results from the Sprites94 aircraft campaign: 1. Red sprites, *Geophys. Res. Lett.*, *22*(10), 1205–1208, doi:10.1029/95GL00583.

Sentman, D. D., E. M. Wescott, R. H. Picard, J. R. Winick, H. C. Stenbaek-Nielsen, E. M. Dewan, D. R. Moudry, and J. Morrill (2003), Simultaneous observations of mesospheric gravity waves and sprites generated by a midwestern thunderstorm, *J. Atmos. Solar-Terr. Phys.*, *65*(5), 537–550, doi:10.1016/S1364-6826(02)00328-0

Shafer, M. A., D. R. MacGorman, and F. H. Carr (2000), Cloud-to-ground lightning throughout the lifetime of a severe storm system in Oklahoma, *Mon. Weather Rev.*, *128*, 1798–1816, doi:10.1175/1520-0493(2000)128<1798:CTGLTT>2.0.CO;2.

Shao, X., and P. Krehbiel (1996), The spatial and temporal development of intracloud lightning, *J. Geophys. Res.*, *101*(D21), 26,641–26,668, doi:10.1029/96JD01803.

Shao, X., C. Rhodes, and D. Holden (1999), RF radiation observations of positive cloud-to-ground flashes, *J. Geophys. Res.*, *104*(D8), 9601–9608, doi:10.1029/1999JD900036.

Soula, S., O. van der Velde, J. Montanya, T. Neubert, O. Chanrion, and M. Ganot (2009), Analysis of thunderstorm and lightning activity associated with sprites observed during the EuroSprite campaigns: Two case studies, *Atmos. Res.*, *91*(2–4), 514–528, doi:10.1016/j.atmosres.2008.06.017.

Soula, S., O. van der Velde, J. Palmieri, J. Montanya, O. Chanrion, T. Neubert , F. Gangneron, Y. Meyerfeld, F. Lefeuvre, and G. Lointier (2010), Characteristics and conditions of production of transient luminous events observed over a maritime storm, *J. Geophys. Res.*, *115*, D16118, doi:10.1029/2009JD012066.

Stanley, M. A. (2000), Sprites and their parent discharges, Ph.D. dissertation, 163 pp., New Mexico Institute of Mining and Technology, Socorro, NM, USA.

Stolzenburg, M., T. C. Marshall, W. D. Rust, E. Bruning, D. R. MacGorman, and T. Hamlin (2007), Electric field values observed near lightning flash initiations, *Geophys. Res. Lett.*, *34*, L04804, doi:10.1029/2006GL028777.

Vadislavsky, E., Y. Yair, C. Erlick, C. Price, E. Greenberg, R. Yaniv, B. Ziv, N. Reicher, and A. Devir (2009), Indication for circular organization of column sprite elements associated with Eastern Mediterranean winter thunderstorms., *J. Atmos. Solar-Terr. Phys.*, *71*, 1835–1839, doi:10.1016/j.jastp.2009.07.001.

Valdivia, J., G. Milikh, and K. Papadopoulos (1997), Red sprites: Lightning as a fractal antenna, *Geophys. Res. Lett.*, *24*(24), 3169–3172, doi:10.1029/97GL03188.

Valine, W. C., and E. P. Krider (2002), Statistics and characteristics of cloud-to-ground lightning with multiple ground contacts, *J. Geophys. Res.*, *107*(D20), 4441, doi: 10.1029/2001JD001360.

Van der Velde, O. A., Á. Mika, S. Soula, C. Haldoupis, T. Neubert, and U. S. Inan (2006), Observations of the relationship between sprite morphology and in-cloud lightning processes, *J. Geophys. Res.*, *111*, D15203, doi:10.1029/2005JD006879.

Wescott, E. M., H. C. Stenbaek-Nielsen, D. D. Sentman, M. J. Heavner, D. R. Moudry, and F. T. S. Sabbas (2001), Triangulation of sprites, associated halos and their possible relation to causative lightning and micrometeors, *J. Geophys. Res.*, *106*(A6), 10,467–10,478, doi:10.1029/2000JA000182.

Williams, E., E. Downes, R. Boldi, W. Lyons, and S. Heckman (2007), Polarity asymmetry of sprite-producing lightning: A paradox?, *Radio Sci.*, *42*, RS2S17, doi:10.1029/2006RS003488.

Yair, Y., R. Aviv, G. Ravid, R. Yaniv, B. Ziv and C. Price (2006), Evidence for synchronicity of lightning activity in networks of spatially remote thunderstorms, *J. Atmos. Sol. Terr. Phys.*, *68*, 1401–1415.

Yair, Y., R. Aviv, and G. Ravid (2009), Clustering and synchronization of lightning flashes in adjacent thunderstorm cells from lightning location networks data, *J. Geophys. Res.*, *114*, D09210, doi:10.1029/2008JD010738.

Yashunin, S. A., E. A. Mareev, and V. A. Rakov (2007), Are lightning M components capable of initiating sprites and sprite halos?, *J. Geophys. Res.*, *112*, D10109, doi:10.1029/2006JD007631.

J. Bech and N. Pineda, Meteorological Service of Catalonia, Barcelona 08029, Spain.

J. Montanyà and O. A. van der Velde, Lightning Research Group, Electrical Engineering Department, Technical University of Catalonia, C/Colom 1, Terrassa, Barcelona 08222, Spain. (oscar.van.der.velde@upc.edu)

S. Soula, Université de Toulouse, Laboratoire d'Aérologie, CNRS, OMP, 14 ave. Edouard Belin, 31400 Toulouse, France.